Inorg. Chem. **2004**, *43*, 6654–6662

Conformational Flexibility of Nickel(II) Benziporphyrins

Marcin Stępień, Lechosław Latos-Grażyński,* and Ludmiła Szterenberg

Department of Chemistry, University of Wrocław, 14 F. Joliot-Curie Street, Wrocław 50 383, Poland

Received June 25, 2004

^{1}H NMR spectra of three paramagnetic Ni(II) complexes of benziporphyrins have been investigated in a broad temperature range. For the *m*- and *p*-benziporphyrin complexes, the line widths of certain signals exhibit an unusual temperature dependence characteristic of a dynamic process. This behavior is interpreted in terms of an equilibrium in which one of the forms is present at a very small concentration and cannot be observed directly. For the benziporphodimethene complex, the two exchanging forms are present at comparable concentrations and can yield separate signals in the slow exchange limit. To account for the observed exchange process, a mechanism is proposed involving the motion of the phenylene moiety. This hypothesis is further explored with DFT modeling, which indicates that the postulated conformers are thermally accessible.

Introduction

Benziporphyrins are a class of porphyrin analogues in which the macrocycle is formally constructed from three pyrrole rings and one benzenoid ring that are connected by meso bridges.[1−4] Although the generic *m*-benziporphyrin (**1**) exhibits no macrocyclic aromaticity,[1,3] other systems, such as *p*-benziporphyrin (**2**)[4] and oxybenziporphyrin,[2] display ring currents comparable to those of regular porphyrins. Coordination chemistry of benziporphyrins has been studied systematically to reveal that these ligands form organometallic complexes with transition metals,[3,5] activate arene C−H bonds toward oxidative substitutions,[3,6] and stabilize weak metal−arene interactions.[4,7]

In a recent paper, we investigated the complexes of meso-arylbenziporphyrins **1**−**3** with Ni(II), Zn(II), Cd(II), and Hg(II) (**4**−MX, **5**−MX, and **6**−MX, Chart 1), showing that, in those species, the metal interacts weakly with the arene, leading to observable effects in the NMR spectra.[7] In the case of the diamagnetic Cd(II) and Hg(II) systems, direct scalar coupling was observed between the spin-active metal nuclei ($^{111/113}$Cd and ^{199}Hg) and the ^{1}H and ^{13}C spins of the proximate C−H fragment of the arene. For the paramagnetic Ni(II) complexes **4**−NiCl, **5**−NiCl, and **6**−NiCl, unusually large chemical shifts were observed. These shifts were explained in terms of a Ni−arene agostic interaction that is responsible for direct spin density transfer to the benzene ring.

The variable-temperature ^{1}H NMR spectra of benziporphyrin Ni(II) complexes, which were recorded during the previous study, revealed anomalous temperature dependence of line widths, suggesting that some exchange phenomena are active in solution. In the present work, these NMR data are analyzed in detail, and an exchange mechanism is proposed that relies on the conformational flexibility of the benziporphyrin ligands.

Results and Discussion

Variable-Temperature NMR Studies of Chloronickel(II) Benziporphyrins. ^{1}H NMR spectra for compounds **4**−NiCl, **5**−NiCl, and **6**−NiCl were analyzed in detail in a previous paper.[7] Importantly, all systems gave Curie plots with only small deviations from linearity, which were interpreted as a small dipolar contribution induced by zero-field splitting (ZFS). T_1 relaxation times were found to be mainly of dipolar origin and provided useful geometrical information. However, the effective T_2' times showed an anomalous temperature dependence for almost all paramagnetically shifted signals.

This unusual line broadening pattern can be most readily appreciated in the case of the 22-H signal of chloronickel-

* To whom the correspondence should be addressed. E-mail LLG@wchuwr.chem.uni.wroc.pl.

(1) Berlin, K.; Breitmaier, E. *Angew. Chem., Int. Ed. Engl.* **1994**, *33*, 1246.
(2) Lash, T. D. *Angew. Chem., Int. Ed. Engl.* **1995**, *34*, 2533.
(3) Stępień, M.; Latos-Grażyński, L. *Chem. Eur. J.* **2001**, *7*, 5113.
(4) Stępień, M.; Latos-Grażyński, L. *J. Am. Chem. Soc.* **2002**, *124*, 3838.
(5) Stępień, M.; Latos-Grażyński, L.; Lash, T. D.; Szterenberg, L. *Inorg. Chem.* **2001**, *40*, 6892.
(6) Stępień, M.; Latos-Grażyński, L. *Org. Lett.* **2003**, *5*, 3379.
(7) Stępień, M.; Latos-Grażyński, L.; Szterenberg, L.; Panek, J.; Latajka, Z. *J. Am. Chem. Soc.* **2004**, *126*, 4566.

10.1021/ic049172d CCC: $27.50
Published on Web 09/23/2004

Chart 1

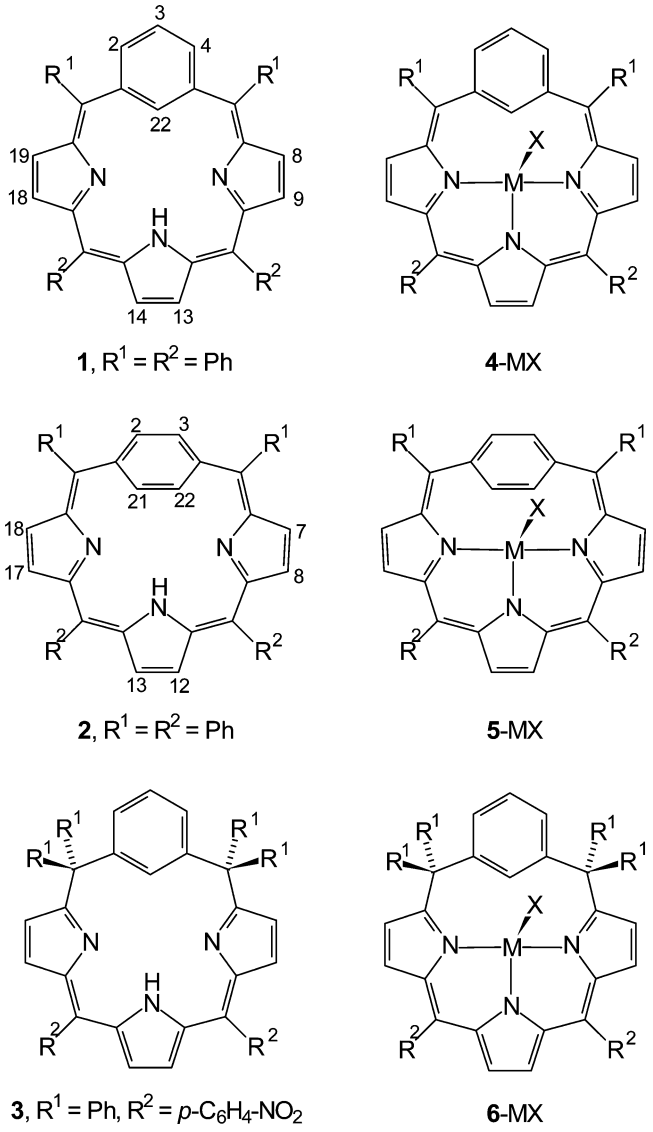

(II) *m*-benziporphyrin, **4**−NiCl. In a paramagnetic compound, the line width of a signal is expected to increase monotonically as the temperature is lowered. When **4**−NiCl is dissolved in chloroform-*d*, the half-width of 22-H is 4.0 kHz at 333 K, and it *decreases* to 1.9 kHz at 293 K (at the 500-MHz base frequency). At lower temperatures, the signal broadens again, reaching a half-width of 4.0 kHz at 213 K. Measurements carried out in a wider temperature range available in toluene-d_8 have shown that heating the sample above 333 K results in a decrease of the 22-H line width, which reaches 2.4 kHz at 373 K.

The temperature dependence of line widths in the ^{1}H NMR spectrum of **4**−NiCl is shown in Figures 1 and 2 (in chloroform-*d* and toluene-d_8 solutions, respectively) for the *m*-phenylene and β-pyrrole signals of **4**−NiCl. The pattern observed for the line width of 22-H is quite well reproduced by the remaining resonances. At this point, it is convenient to define temperature regions (denoted by Roman numerals), wherein the slope of the line width dependence takes different signs. The low-temperature region I has in each case a positive slope and is followed by region II (negative slope);

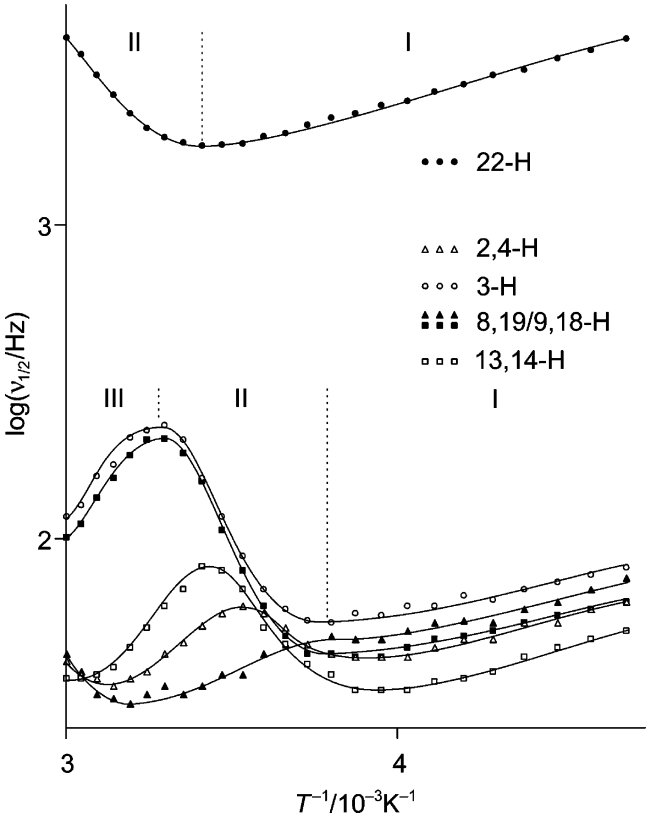

Figure 1. Temperature dependence of line widths in the ^{1}H NMR spectrum of **4**−NiCl (chloroform-*d*, 213−333 K). Continuous lines are for illustrative purposes only.

region III (positive slope); and, finally, region IV (negative slope), which is observed at highest temperatures (in toluene-d_8, Figure 2).

In Figures 1 and 2, logarithms of $\nu_{1/2}$ are plotted against T^{-1}, which has often been found to yield a linear plot for a paramagnetic species in the absence of chemical exchange.[8,9] Moreover, the slope should be positive and approximately equal for all protons in the molecule. Indeed, this general rule holds sufficiently well for the low-temperature region of the chloroform-*d* data (region I, Figure 1). However, noticeable curvature is found in toluene-d_8, suggesting an influence of increasing viscosity or an interaction with the solvent. Actually, depending on the system, the relationship between log $\nu_{1/2}$ and T^{-1} can be quite complex and not necessarily linear.[10] Linear extrapolation of the nonexchange region I should therefore be applied with considerable caution. Consequently, the toluene-d_8 data will be analyzed only qualitatively.

It is essential to add that basically linear dependencies of log $\nu_{1/2}$ vs T^{-1} were previously observed for several paramagnetic nickel(II) heteroporphyrins and carbaporphyrins.[11−16] To substantiate those findings, appropriate ^{1}H NMR data for nickel(II) 21-oxaporphyrin[14] and nickel(II) dimethylated-inverted porphyrin[13] were reexamined in the course of these investigations.

(8) Satterlee, J. D.; La Mar, G. N.; Bold, T. J. *J. Am. Chem. Soc.* **1977**, *99*, 1088.
(9) La Mar, G. N.; Sherman, E. O. *J. Am. Chem. Soc.* **1970**, *92*, 2691.
(10) Bertini, I.; Luchinat, C. *Coord. Chem. Rev.* **1996**, *150*, 1.

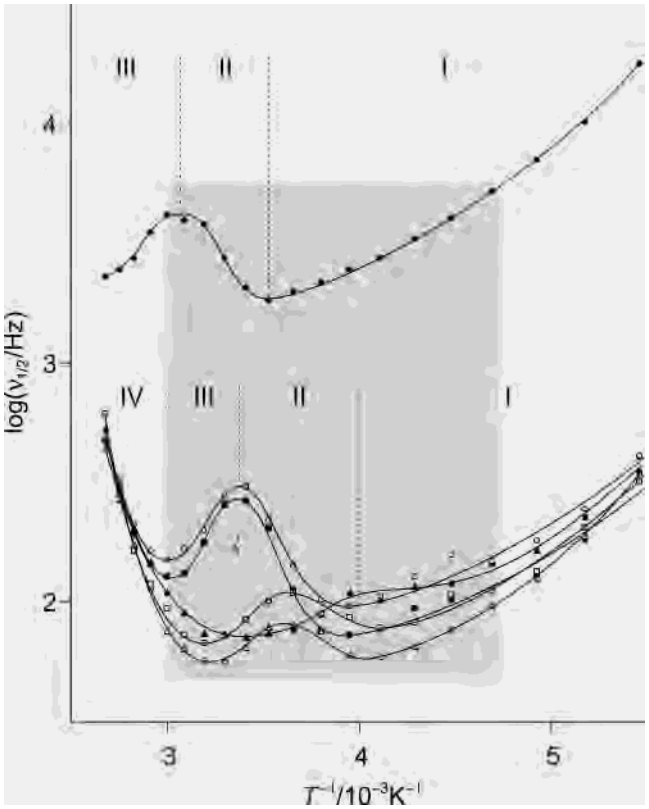

Figure 2. Temperature dependence of line widths in the ^{1}H NMR spectrum of **4**−NiCl (toluene-d_8, 183−373 K). Continuous lines are for illustrative purposes only. The gray rectangle corresponds to the plotting limits of Figure 1.

The position and height of the conspicuous maximum separating regions II and III varies among the resonances but is virtually independent of the choice of solvent. The maximum is particularly strongly shifted to high temperatures in the case of signal 22-H. In all cases, the accompanying local minima (I/II and III/IV) are shifted in a similar fashion.

The temperature dependence of line widths was also investigated for the signals of chloronickel(II) *p*-benziporphyrin, **5**−NiCl (Figure 3, dichloromethane-d_2). Departures from linearity are significant, especially for signals 12,13-H and 2,3-H, and resemble the profiles obtained for **4**−NiCl. The line width of 21,22-H could not be measured in the whole temperature range. At higher temperatures, the broad 21,22-H resonance has a small positive shift and overlaps with the signals of diamagnetic impurities. At low temperatures (below 223 K), additional signals of low intensity appear in the ^{1}H NMR spectrum of **5**−NiCl, corresponding to at least one additional species. It is uncertain whether this

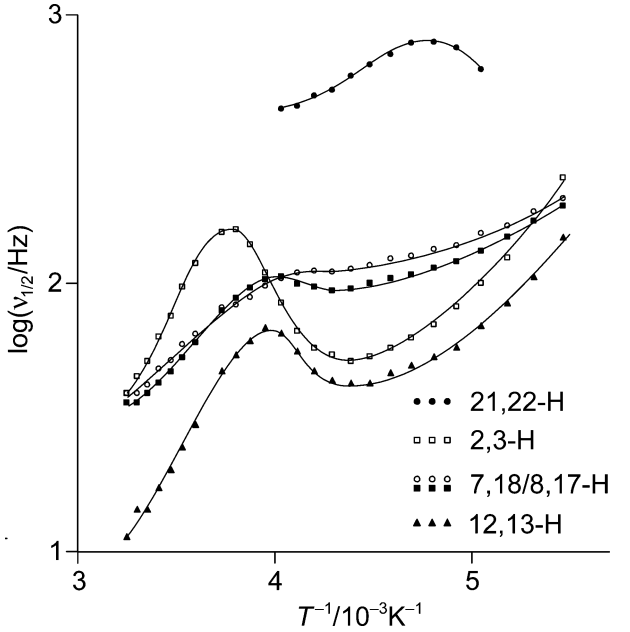

Figure 3. Temperature dependence of line widths in the ^{1}H NMR spectrum of **5**−NiCl (chloroform-*d*, 213−333 K). Continuous lines are for illustrative purposes only.

species is responsible for the dynamic broadening observed at higher temperatures.

As the temperature is lowered, the ^{1}H NMR spectrum of **6**−NiCl undergoes significant dynamic broadening, which finally results in the decoalescence of all signals. At 168 K, two forms can be observed in comparable concentrations (Figure 4). Pairs of corresponding resonances have similar shifts with the notable exception of 22-H, where the shift difference is as large as 150 ppm (which corresponds to ca. 80 ppm at 298 K).

Analysis of the Dynamic Broadening in 4−NiCl. The observed temperature profiles (regions I−III) correspond to an exchange process between two paramagnetic species A and B, of which one is significantly less populated ($P_A \gg P_B$) and thus impossible to observe directly.[8,10,17] The dynamic process is slow in region I, and the observed dependence can be attributed solely to paramagnetic broadening and extrapolated into regions II and III.[8] However, the negative slope observed in the high-temperature region IV (toluene-d_8) is not associated with the exchange between A and B[17] and suggests the presence of another dynamic process that has a higher activation energy. A third species C must therefore be involved, with $P_A \gg P_C$ in the studied range of temperatures. The following discussion will concentrate on the analysis of region II, which corresponds to the limit of slow exchange between A and B.

In the slow exchange limit, the following condition is fulfilled

$$\pi^2(\nu_{A,i} - \nu_{B,i})^2 \gg T_{2,B,i}^{-2}, \tau_B^{-2} \qquad (1)$$

(11) Latos-Grażyński, L. *Inorg. Chem.* **1985**, *24*, 1681.
(12) Lisowski, J.; Latos-Grażyński, L.; Szterenberg, L. *Inorg. Chem.* **1992**, *31*, 1933.
(13) Chmielewski, P. J.; Latos-Grażyński, L.; Głowiak, T. *J. Am. Chem. Soc.* **1996**, *118*, 5690.
(14) Chmielewski, P. J.; Latos-Grażyński, L.; Olmstead, M. M.; Balch, A. L. *Chem. Eur. J.* **1997**, *3*, 268.
(15) Chmielewski, P. J.; Latos-Grażyński, L. *Inorg. Chem.* **1998**, *37*, 4179.
(16) Latos-Grażyński, L. Core Modified Heteroanalogues of Porphyrins and Metalloporphyrins. In *The Porphyrin Handbook*; Kadish, K. M., Smith, K. M., Guilard, R., Eds.; Academic Press: New York, 2000; Vol. 2, Chapter 14, pp 361−416.
(17) Swift, T. J. The Paramagnetic Linewidth. In *NMR of Paramagnetic Molecules. Principles and Applications*; La Mar, G. N., Horrocks, W. D., Jr., Holm, R. H., Eds.; Academic Press: New York, 1973; Chapter 2, pp 53−83.

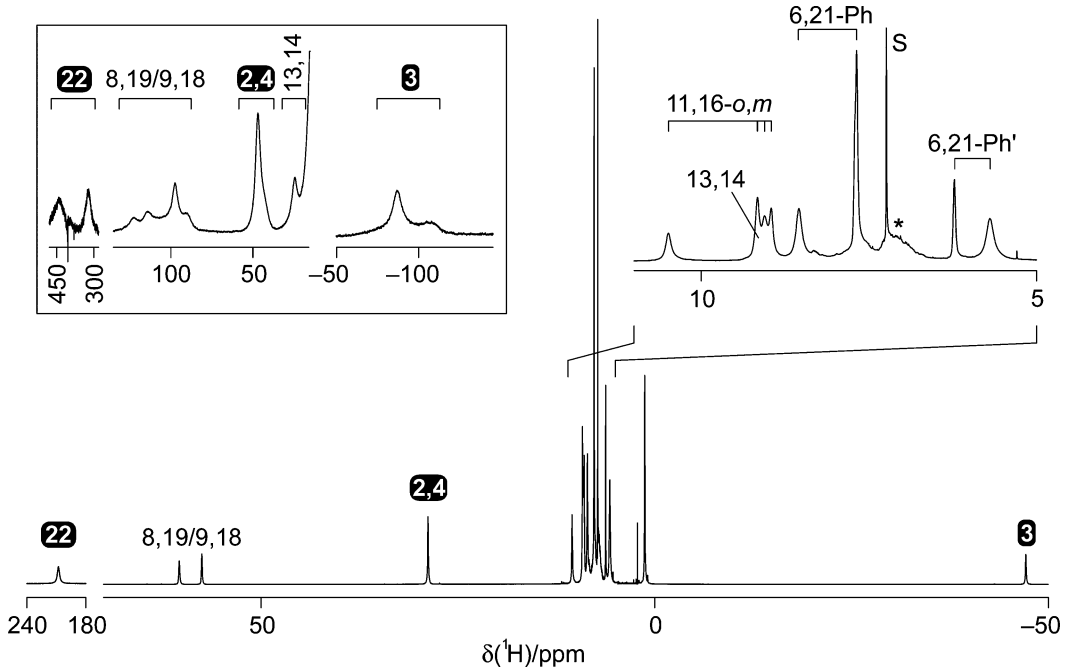

Figure 4. ^{1}H NMR spectrum of **6**−NiCl-d_6 (298 K, chloroform-*d*). The compound was selectively deuterated in positions 8,19-H, 9,18-H, and 13,14-H, and the respective signals have reduced intensities. The signals in the diamagnetic region (right inset) have been assigned using TOCSY connectivities; the observed number of lines is smaller than expected because of accidental overlaps. The left inset shows the spectrum of **6**−NiCl-d_6 obtained at low temperature (168 K, dichloromethane-d_2).

where $\nu_{A,i} - \nu_{B,i}$ is the chemical shift difference of signal i between species A and B, $T_{2,B,i}$ is the corresponding spin−spin relaxation time for species B in the absence of exchange, and τ_B is the preexchange lifetime for B.[17] The line width $\nu_{1/2}$ of signal i in species A is then given by

$$\pi\nu_{1/2,A,i} = T'_{2,A,i}{}^{-1} = T_{2,A,i}{}^{-1} + \tau_A{}^{-1} \qquad (2)$$

where $T_{2,A,i}$ and τ_A are defined analogously. The above equation can be rearranged to

$$\nu_{1/2,A,i}(\text{observed}) - \nu_{1/2,A,i}(\text{extrapolated}) = 1/\pi\tau_A \qquad (3)$$

where $\nu_{1/2,A,i}$(extrapolated) is now the line width in the absence of exchange. This quantity can be obtained experimentally by determining $\nu_{1/2,A,i}$ over a wide temperature range in the region of no exchange and extrapolating into the exchange region as discussed above.

As the minor form B is expected to be paramagnetic, even for similar $T_{2,B,i}$ values, the value of $\pi^2(\nu_{A,i} - \nu_{B,i})^2$ can vary considerably as a result of the large spread of shifts and their temperature dependence. Thus condition 1, applicable in the slow exchange limit, and a corresponding condition for the fast exchange limit (not discussed) are met by each resonance pair in a different temperature range, accounting for the different positions of the extremes in the $\{\nu_{1/2,A,i}\}$ profiles. This effect enables the determination of $\{\tau_A{}^{-1}\}$ in a wider temperature range, as the values obtained for different resonances should combine into a single linear plot.

Figure 5 shows the Eyring plot for region II of the **4**−NiCl data collected in chloroform-*d*. Data points corresponding to region II are included (one of the signals, which showed little dynamic broadening, was omitted). Departures from linearity indicate that, as expected, the slow exchange condition is fulfilled only at lower temperatures. However, the linear parts of the profiles coincide to form a straight line, from which activation parameters can be calculated. The values $\Delta H^{\ddagger} = 63$ kJ/mol and $\Delta S^{\ddagger} = 20$ J/mol·K yield $\Delta G^{\ddagger} = 57$ kJ/mol (298 K). This value is in the range found for various dynamic processes observed in porphyrins, including rotation of *meso*-aryl substituents and macrocyclic inversion.[18−20]

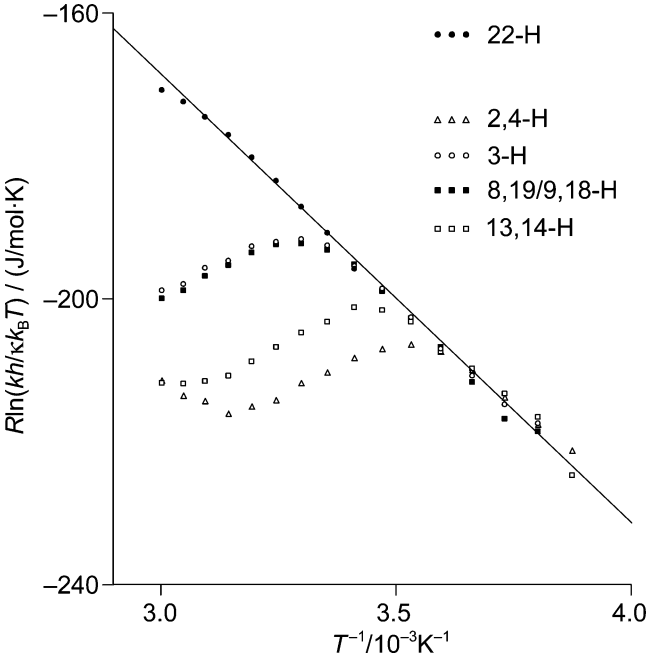

Figure 5. Eyring plot for pertinent ^{1}H NMR signals of **4**−NiCl obtained from the chloroform-*d* data (Figure 1, one of the 8,19/9,18-H signals was omitted). The straight line corresponds to $\Delta H^{\ddagger} = 63$ kJ/mol and $\Delta S^{\ddagger} = 20$ J/mol·K. Data points included in the (unweighted) fitting were selected by hand.

At lower temperatures, the contribution of dynamic broadening to the observed line width decreases (also because of the increasing paramagnetic line width), which adversely affects the accuracy of τ_A determination. The activation parameters given above might therefore be slightly biased.

It should be noted that, for signal 22-H, region III is shifted to higher temperatures relative to the remaining signals. This implies that the chemical shift difference between the exchanging species is significantly greater for 22-H than for other signals, as τ_A is proportional to $(\nu_{A,i} - \nu_{B,i})^2$ in the fast exchange limit.[17] No quantitative treatment is possible, as temperature regions III of 22-H and the remaining signals do not overlap.

The high-temperature region IV, observed for **4**−NiCl in toluene-d_8 solutions, is characterized by negative slope and probably corresponds to the onset of another dynamic process. As reported earlier, heating **4**−NiCl in MeCN/$CHCl_3$ results in the loss of a HCl molecule and formation of a Ni−C bond.[7] The process activated in region IV can therefore be conjectured to have a dissociative character.

Several mechanisms can be proposed to account for the observed dynamic behavior of **4**−NiCl (regions II and III) and the remaining nickel complexes:

1. One possibility is dissociation or association of an axial ligand. This hypothesis can be dismissed for the following reasons: (a) Dynamic broadening observed for **4**−NiCl is not affected by a large excess of chloride ions (introduced to the chloroform-*d* solution in the form of benzyltriethylammonium chloride), which should influence the equilibrium between forms A and B. (b) Changes in the structure of the macrocyclic ligand (e.g., *m*-benziporphyrin vs *m*-benziporphodimethene) should not have a strong effect on axial ligation.

2. Changes in the metal−arene bonding (e.g., dynamic formation and breaking of a M−C σ bond) should be ineffective in the case of chloronickel(II) *p*-benziporphyrin (**5**−NiCl) where the orientation of the arene with respect to the nickel center is much less favorable than in **4**−NiCl.

3. A third possibility is conformational dynamics involving puckering of the benziporphyrin macrocycle, rotation of *meso*-aryl rings, or both. This idea is elaborated in the following sections.

Flexibility of Benziporphyrin Ligands. Benziporphyrin macrocycles are generally more flexible than regular porphyrins, as can be judged from the puckered structures observed in the solid state for free bases and their complexes.[3,4,7,21] This is a result of the loss (or decrease) of macrocyclic aromaticity combined with the steric constraints generated by the introduction of a phenylene ring to the macrocyclic structure.

Scheme 1

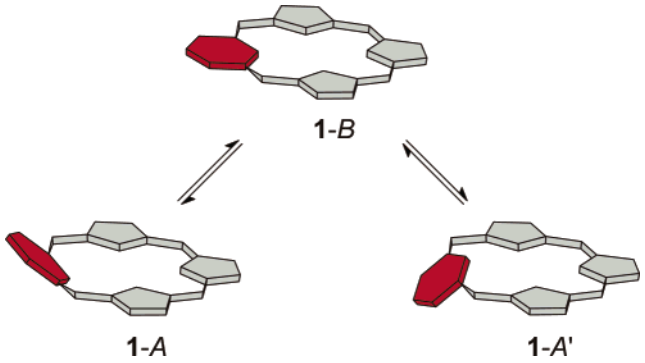

Scheme 2

Whereas the reported ^{1}H and ^{13}C NMR spectra of tetraphenyl-*m*-benziporphyrin (**1**) correspond to an effectively planar structure,[3] variable-temperature data recorded for **1** indicate that some conformational equilibrium takes place in solution. Chemical shifts of all signals show a distinct temperature dependence. For instance, in a dichloromethane-d_2 solution, signal 22-H moves from 7.3 ppm at 298 K to 6.9 ppm at 180 K, which is accompanied by gradual broadening of the spectrum (the slow exchange limit could not be achieved on a 300-MHz spectrometer). In toluene-d_8, the same signal experiences a shift change from 7.9 to 7.5 ppm (298 to 198 K), and again, significant dynamic broadening is observed at lower temperatures.

Possibly, the equilibrium involves an exchange between a nonplanar conformation (**1**−*A* and **1**−*A*′, Scheme 1) and a planar one (**1**−*B*). The nonplanar form corresponds to the solid-state geometry observed for 22-acetoxy-*m*-benziporphyrin.[3] It can be argued that the latter conformation is induced by the bulk of the 22-OAc substituent, but a preliminary structure of the 22-unsubstituted species **1** exhibited an identical degree of nonplanarity.[22] On the other hand, the formation of square-planar nickel(II), palladium(II), and platinum(II) *m*-benziporphyrins with a M−C bond supports the feasibility of the planar structure **1**−*B*.[3,7]

In the case of *p*-benziporphyrin (**2**), the planar conformation of the macrocycle is probably unavailable because of steric congestion inside the molecule. However, *p*-benziporphyrin exchanges between two degenerate nonplanar conformations **2**−*A* and **2**−*A*′ in a seesaw fashion (Scheme 2), which leads to spectacular effects in the variable-temperature ^{1}H NMR spectra.[4]

Macrocyclic inversions discussed here for benziporphyrins are not, in fact, uncommon in the porphyrin world. Dynamic processes have previously been reported for sterically

(18) Barkigia, K. M.; Berber, M. D.; Medforth, C. J.; Renner, M. W.; Smith, K. M. *J. Am. Chem. Soc.* **1990**, *112*, 8851.
(19) Medforth, C. J. NMR Spectroscopy of Diamagnetic Porphyrins. In *The Porphyrin Handbook*; Kadish, K. M., Smith, K. M., Guilard, R., Eds.; Academic Press: New York, 2000; Vol. 5, Chapter 35, pp 1−80.
(20) Medforth, C. J.; Berber, M. D.; Smith, K. M.; Shelnutt, J. A. *Tetrahedron Lett.* **1990**, *31*, 3719.
(21) Stępień, M.; Latos-Grażyński, L. *Inorg. Chem.* **2003**, *42*, 6183.
(22) Stępień, M. Ph.D. Thesis, Uniwersytet Wrocławski, 2003.

Scheme 3

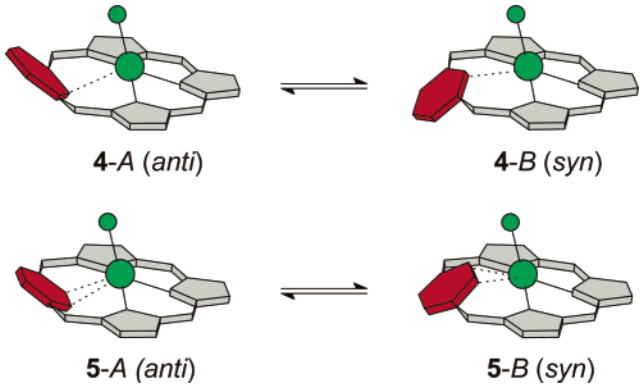

crowded porphyrins,[18−20,23] tetraarylsapphyrins and their heteroanalogues,[24−28] and 21,23-ditelluraporphyrin.[29]

Conformational Dynamics of Benziporphyrin Complexes. DFT Studies. In metal complexes **4**−MX and **5**−MX, the preferred conformation of the macrocycle has the phenylene ring tilted away from the metal center with the inner CH bonds and the axial MX bond in an anti orientation (**4**−*A* and **5**−*A*, Scheme 3), as confirmed by X-ray structures of **4**−NiCl, **4**−CdCl, **5**−NiCl, and **5**−CdCl.[4,7] However, it is possible that minute amounts of syn conformers (**4**−*B* and **5**−*B*) might be present in solution and rapidly equilibrate with the respective anti forms.

To investigate whether the syn conformers are indeed energetically available, we performed a series of DFT calculations of chlorozinc(II) and chlorocadmium(II) systems. The chlorozinc complexes were chosen as a closed-shell substitute for the original paramagnetic nickel(II) species to simplify calculations.

It is evident from inspection of molecular models that the torsional freedom of 6,21-aryl substituents in **4**−MX (5,20-aryls in **5**−MX) can increase the number of distinct conformations. Variable-temperature NMR data recorded for the Ni(II) complexes show that the rotations of *meso*-aryls are much less obstructed for the substituents closer to the phenylene moiety (6,21 in **4**−MX and 5,20 in **5**−MX).

Using molecular mechanics and semiempirical calculations, we selected six different geometries of **4**−ZnCl and subjected them to a DFT optimization at the B3LYP/LANL2DZ level of theory. The final geometries, **4**−ZnCl−*A* through **4**−ZnCl−*F*, are shown in Figure 6. In each case, a genuine energy minimum was obtained. For comparison, an analogous series of conformers, **4**−CdCl−*A* through **4**−ZnCl−*F*, were optimized. In each case, the conformation of the *m*-benziporphyrin macrocycle resembled that of the Zn(II) counterpart.

Selected geometrical parameters and relative energies for **4**−ZnCl and **4**−CdCl are given in Table 1. For each system, there are three anti (*A*, *C*, *E*) and three syn (*B*, *D*, *F*) conformers that differ in the orientation of the 6,21-phenyl rings. Each conformer can be uniquely characterized by the signs of the torsion angles $\varphi_1-\varphi_4$, as defined in the footnote of Table 1. The distinction between anti and syn conformers is made on the basis of the signs of φ_1 and φ_2 ($^{+}\varphi_1{}^{-}\varphi_2$ for anti and $^{-}\varphi_1{}^{+}\varphi_2$ for syn), whereas the remaining two angles define the orientation of the 6,21-phenyls. Conformers *A*−*D* contain a symmetry plane, which is absent in the chiral structures E and F. The enantiomeric forms *E*′ and *F*′, which might also participate in the dynamic equilibria, are omitted in Figure 6 and Table 1.

Conformers **4**−ZnCl−*A* and **4**−CdCl−*A* correspond to the solid-state geometry found for **4**−CdCl[7] and, as could be expected, have the lowest energies. The energy orderings of the anti conformers in the Zn and Cd series are the same, namely, $E_A < E_E < E_C$. However, the ordering of the syn forms differs remarkably between **4**−ZnCl and **4**−CdCl. The D form, which is characterized by particularly short M···H(22) distances (2.313 Å for **4**−ZnCl and 2.380 Å for **4**−CdCl), is the lowest-energy syn conformer of **4**−ZnCl and the highest-energy syn conformer of **4**−CdCl. The ordering is therefore $E_D < E_B < E_F$ for the Zn species and $E_B < E_F < E_D$ for the Cd species. In the former series, however, the energy differences are very small.

The introduction of the bulkier Cd(II) ion causes an additional energy increase in the syn conformers (*B*, *D*, and *F*) relative to the anti conformers with similar orientation of the 6,21-phenyl rings (*A*, *C*, and *E*, respectively). This effect is particularly pronounced for the *C*−*D* pair: $E_D - E_C$ is −2.35 kcal/mol for **4**−ZnCl but +3.50 kcal/mol for **4**−CdCl.

The angle between the phenylene plane and the plane of the three pyrrolic nitrogens (C_6/N_3) is markedly dependent on the orientation of the adjacent *meso*-phenyl rings, which, in turn, affects the M···C and M···H distances in the coordination core. The importance of meso substituents in stabilizing the overall conformation of the macrocycle is even more evident when the previously published data on meso-unsubstituted **4**−CdCl are considered.[7] The C_6/N_3 angle obtained for that DFT-optimized structure was 23°, i.e., much smaller than the X-ray structural value of 52°. When the meso substituents are introduced into the calculation, the C_6/N_3 angle becomes 48°, which nicely agrees with the X-ray data.

The *A* and *B* conformers optimized by DFT for complexes **5**−ZnCl, **5**−CdCl, **6**−ZnCl, and **6**−CdCl (Figure 7, Table 1) were selected in a preliminary PM3 calculation as the lowest-energy anti (*A*) and syn (*B*) species. For the *p*-benziporphyrin complexes, the energy differences are slightly larger than for the *m*-benziporphyrin case.

The geometries obtained for the selected conformers of **6**−ZnCl and **6**−CdCl are significantly twisted. In fact, no geometry including a symmetry plane could be obtained as an energy minimum in the PM3 calculations. Apparently,

(23) Hobbs, J. D.; Majumder, S. A.; Luo, L.; Sickelsmith, G. A.; Quirke, J. M. E.; Medforth, C. J.; Smith, K. M.; Shelnutt, J. A. *J. Am. Chem. Soc.* **1994**, *116*, 3261.
(24) Chmielewski, P. J.; Latos-Grażyński, L.; Rachlewicz, K. *Chem. Eur. J.* **1995**, *1*, 68.
(25) Rachlewicz, K.; Sprutta, N.; Chmielewski, P. J.; Latos-Grażyński, L. *J. Chem. Soc., Perkin Trans. 2* **1998**, 969.
(26) Rachlewicz, K.; Latos-Grażyński, L.; Gebauer, A.; Vivian, A.; Sessler, J. L. *J. Chem. Soc., Perkin Trans. 2* **1999**, 2189.
(27) Szterenberg, L.; Latos-Grażyński, L. *THEOCHEM* **1999**, *490*, 33.
(28) Szterenberg, L.; Latos-Grażyński, L. *J. Phys. Chem. A* **1999**, *103*, 3302.
(29) Pacholska, E.; Latos-Grażyński, L.; Ciunik, Z. *Angew. Chem., Int. Ed.* **2001**, *40*, 4466.

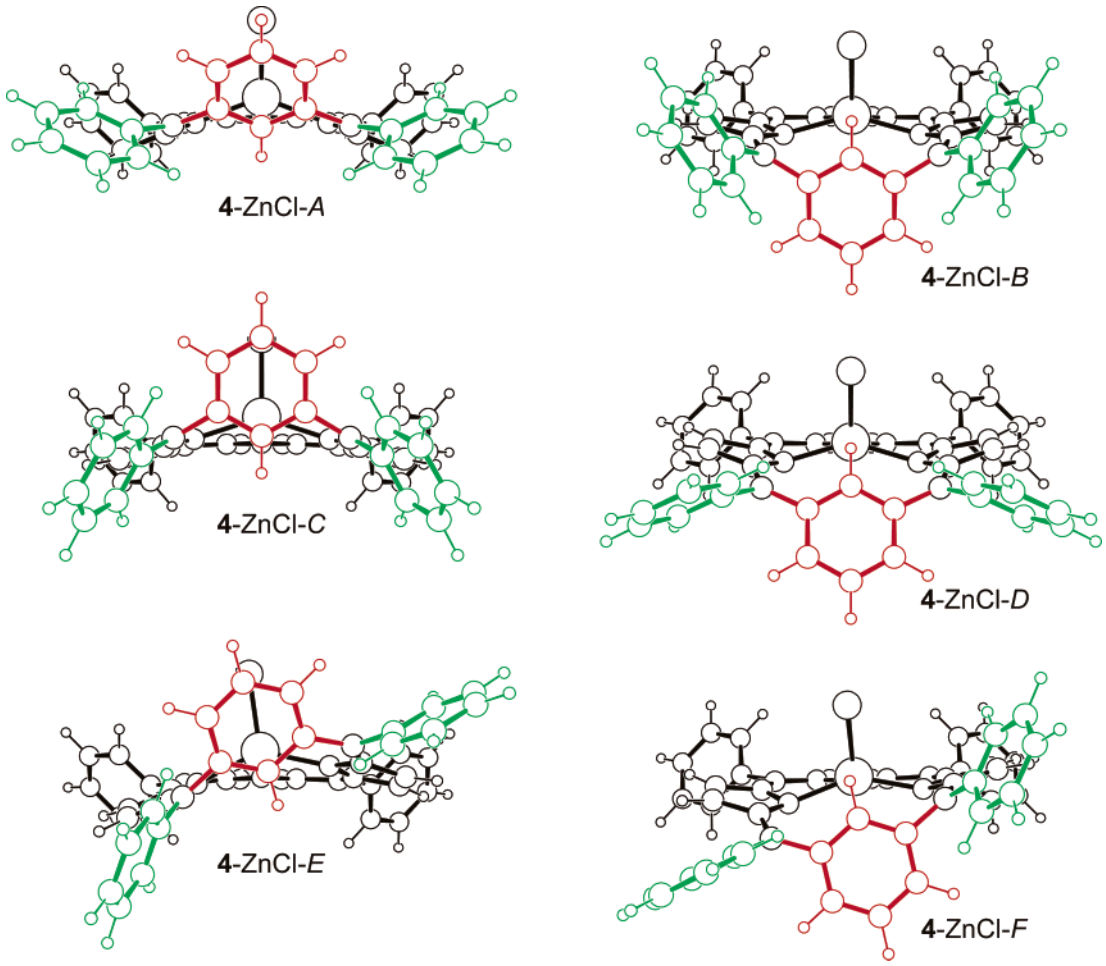

Figure 6. Geometries of the zinc complexes **4**−ZnCl obtained in a DFT optimization (LANL2DZ). The phenylene rings are shown in red, and the 6,21-phenyl substituents are in green.

the twist helps increase the separation between the 6,21-phenyl rings flanking the H(22) atom. Interestingly, on going from **6**−ZnCl to **6**−CdCl, the relative energy of the syn conformer decreases. The modest value of 3.44 kcal/mol obtained for **6**−CdCl−*B* indicates that the coordination core of the benziporphodimethene **3** is more spacious than that of *m*-benziporphyrin **1**.

On the basis of the NMR data and DFT calculations, a mechanism can be proposed for the dynamics of **4**−NiCl, in which the most stable conformer *A* dominates in the whole temperature range. It is accompanied by a very small amount of one of the other conformers *B*−*F*. The question arises whether the minor form differs from A by the orientation of *m*-phenylene and 6,21-Ph substituents.

As noted earlier, the chemical shift difference for 22-H in the two exchanging species should be significantly greater than for the remaining signals. As shown in a previous paper,[7] the 22-H shift is transferred directly through the Ni···H agostic bond and is strongly dependent on the geometry of the agostic interaction. Therefore, it can be argued that the other species involved in the main exchange process must differ considerably from A with regard to the metal−arene bonding. The agostic interaction, as quantified by the distances M···H and M···C and the M−H−C angle (Table 1), is indeed affected by the conformational changes under study. For instance, in the **4**−ZnCl conformers, the calculated M···H distance ranges from 2.31 to 3.07 Å, and the M−H−C angle from 70° to 93°. Interestingly, the geometrical effect of *meso*-aryl rotation is similar to that exerted by the syn−anti transformation, i.e., it is impossible to tell from the DFT data which of these two processes is responsible for the observed dynamic behavior.

The syn−anti exchange mechanism is supported by the observation that the dynamic broadening depends on the internal substitution of the benziporphyrin macrocycle. Examination of the variable-temperature data obtained for chloronickel(II) 6,11,16,21-tetraphenyl-22-acetoxy-*m*-benziporphyrin[21] shows that, for this species, virtually no dynamic broadening is observed. The presence of the 22-acetoxy substituent in the coordination core is likely to hinder the formation of syn conformers.

The proposed mechanism should, in principle, be operative not only in nickel(II) benziporphyrins but also in other metal complexes of these ligands. However, for diamagnetic systems, such as Zn(II) or Cd(II) species, the chemical shift differences between the exchanging conformers are certainly much smaller than for the Ni(II) analogues. As a consequence, the processes might be undetectable by ^{1}H NMR in the available range of temperatures. In addition, as discussed above for **4**−ZnCl and **4**−CdCl, the ionic radius of the

Table 1. Relative Energies and Selected Geometrical Parameters of the DFT-Optimized Structures of the Zn and Cd Benziporphyrins

		distances/Å		angles/deg		torsion angles/deg[b,c]			
structure	ΔE,[a] kcal/mol	M···C(22)	M···H(22)	MH(22)C(22)	C_6/N_3[d]	φ_1	φ_2	φ_3	φ_4
4−ZnCl−*A*	0.00 (0.00)	2.812	2.653	86.87	50.9	43.2	−43.2	50.1	−50.1
4−ZnCl−*B*	4.87 (4.77)	2.937	2.922	80.10	−89.9	−89.6	89.6	28.8	−28.8
4−ZnCl−*C*	7.15 (7.10)	2.891	3.070	70.29	72.7	75.5	−75.5	−32.8	32.8
4−ZnCl−*D*	4.80 (4.81)	2.816	2.313	73.96	−62.0	−49.0	49.0	−53.1	53.1
4−ZnCl−*E*	3.45 (3.42)	2.833	2.862	77.52	62.5	46.1	−74.1	43.7	27.6
4−ZnCl−*F*	5.39 (5.30)	2.834	2.553	93.33	−71.4	−80.1	57.6	25.9	46.5
4−CdCl	n/a	2.722(5)	2.74(5)	78.55	51.7	53.5	−48.3	40.9	−41.7
(X-ray)[e]		2.709(5)	2.59(5)	87.14	52.0	47.5	−50.5	44.3	−44.2
4−CdCl−*A*	0.00	2.806	2.751	81.58	48.1	45.4	−45.4	48.1	−47.8
4−CdCl−*B*	6.88	2.873	2.906	77.47	−86.0	−97.3	97.3	27.0	−27.0
4−CdCl−*C*	6.78	2.907	3.221	63.68	72.1	79.6	−79.6	−32.8	32.8
4−CdCl−*D*	10.28	2.799	2.380	79.15	−55.2	−59.6	59.6	−50.1	50.1
4−CdCl−*E*	3.77	2.837	2.989	71.44	61.1	51.3	−76.5	41.9	30.5
4−CdCl−*F*	9.19	2.796	2.642	86.48	−80.2	−90.2	73.4	25.5	44.2
		M−C(21/22)	M−H(21/22)	MH(21)C(21) MH(22)C(22)					
5−ZnCl−*A*	0.00 (0.00)	2.918	3.185	66.05	43.2	31.0	−31.1	45.5	−45.5
		2.919	3.186	66.05					
5−ZnCl−*B*	6.98 (7.08)	2.726	2.786	75.54	−58.1	−38.3	38.3	−43.9	43.9
		2.726	2.786	75.54					
5−CdCl	n/a	2.748(2)	3.06(2)	79.7	44.5	39.2	−34.5	37.9	−41.9
(X-ray)[f]		2.762(2)	3.08(2)	80.1					
5−CdCl−*A*	0.00	2.948	3.295	62.09	45.0	33.2	−33.4	43.1	−42.7
		2.950	3.300	61.99					
5−CdCl−*B*	8.77	2.707	2.805	73.63	−66.2	−46.0	46.0	−43.7	43.7
		2.707	2.805	73.63					
		M−C(22)	M−H(22)	MH(22)C(22)					
6−ZnCl−*A*	0.00 (0.00)	2.764	2.879	73.00	68.9	49.0	−99.1	−49.1	−13.8
								−70.6	64.1
6−ZnCl−*B*	5.27 (5.11)	2.883	2.709	87.98	−83.9	−100.4	68.8	53.4	−60.1
								−18.7	−63.2
6−CdCl−*A*	0.00	2.769	3.016	66.53	68.6	52.9	−102.0	−50.7	−9.4
								−68.9	66.7
6−CdCl−*B*	3.44	2.851	2.750	84.09	−90.9	−107.0	81.0	58.2	−55.1
								−14.3	−71.1

[a] Energies relative to the most stable conformer. Values in parentheses were calculated with the ZPV contribution included. [b] Torsion angles in are defined as follows. **4**−MX, **6**−MX: φ_1, C(20)−C(21)−C(1)−C(22); φ_2, C(22)−C(5)−C(6)−C(7); φ_3, C(1)−C(21)−C_{ipso}−C_{ortho}; φ_4, C(5)−C(6)−C_{ipso}−C_{ortho}. **5**−MX: φ_1, C(19)−C(20)−C(1)−C(21); φ_2, C(22)−C(4)−C(5)−C(6); φ_3, C(1)−C(20)−C_{ipso}−C_{ortho}; φ_4, C(4)−C(5)−C_{ipso}−C_{ortho}. The angles with smaller absolute values are chosen for φ_3 and φ_4. Numbering follows Chart 1; the axial ligand pointing toward the viewer). In **5**−MX conformers, proximal phenylene atoms are always given numbers 21 and 22. [c] For **6**-MX, the top values of φ_3 and φ_4 correspond to the Ph substituents syn to the Cl ligand. [d] Angle between the phenylene mean plane and the plane of N(23)−N(24)−N(25) atoms (positive for anti and negative for syn conformers). [e] Data from ref 7. Parameters correspond to two symmetry-independent molecules. [f] Data from ref 7.

coordinated metal has an evident effect on the relative stabilities of the conformers and probably also on the activation barrier. Thus, the equilibrium constant and reaction rate might be strongly influenced by the choice of metal ion.

It is possible that the syn−anti mechanism is also operative in the case of complexes **5**−NiCl and **6**−NiCl. For the latter species, the two forms are present in comparable concentrations and yield separate ^{1}H NMR signals at low temperatures. The large difference in chemical shifts recorded for 22-H (150 ppm at 168 K) indicates that the orientation of the phenylene with respect to the paramagnetic center differs significantly in the two conformers. The data obtained for **5**−NiCl are not conclusive, but the presence of exchange is evident.

Conclusion

In this report, we have described a spectroscopic and theoretical analysis of the conformational properties of benziporphyrin complexes. The weak metal−arene interaction in these systems is insufficient to make the structure rigid, and the complexes partially retain the flexibility of the free macrocycles. In the case of *m*- and *p*-benziporphyrin nickel complexes, the dynamic character can be inferred from line broadening patterns followed by the paramagnetically shifted lines. Of the two exchanging forms, which differ in the orientation of the phenylene ring (anti versus syn), one is present in a very small concentration and cannot be observed directly. For the analogous *m*-benziporphodimethene complex, the two forms have comparable concentrations and give separate sets of signals at low temperatures.

The present work shows that the metal complexes of porphyrinoids need not always be structurally static. As a consequence, the spectral pattern observed for some systems might be a weighted average of several exchanging conformations and not compare directly to the solid-state geometry. Additional precautions are therefore needed during any quantitative analysis of paramagnetic NMR data for these complexes.

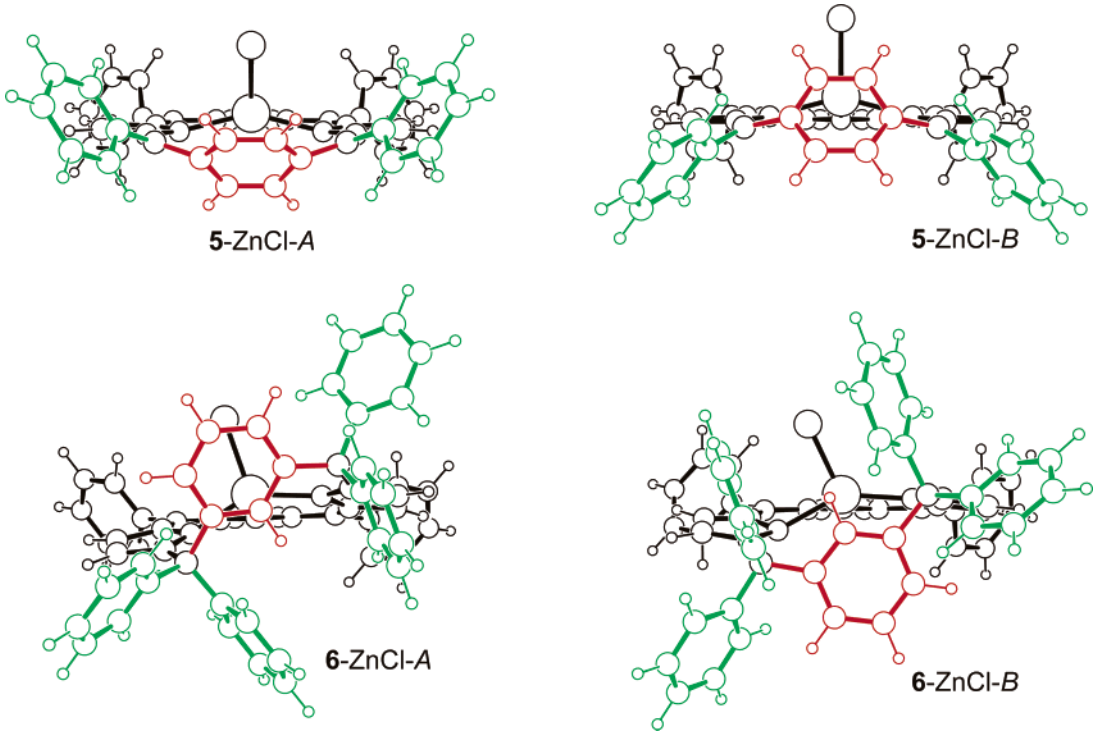

Figure 7. Geometries of the zinc complexes **5**−ZnCl (top) and **6**−ZnCl (bottom) obtained in a DFT optimization (LANL2DZ). The phenylene rings are shown in red, and the 6,21-phenyl substituents are in green.

Experimental Section

Materials. 6,11,16,21-Tetraphenyl-*m*-benziporphyrin (**1**), 5,10,-15,20-tetraphenyl-*p*-benziporphyrin (**2**), 11,16-Bis(4-nitrophenyl)-6,6,21,21-tetraphenyl-*meta*-benzi-6,21-porphodimethene (**3**), and their nickel(II) complexes (**4**−**6**) were obtained as previously described.[3,4,7]

NMR Spectroscopy. NMR spectra were recorded on Bruker Avance 500 and AMX 300 spectrometers (with ^{1}H base frequencies of 500.13 and 300.13 MHz, respectively). Spectra were referenced to residual solvent signals.

Paramagnetically shifted spectra were recorded with fast recycle times (usually below 100 ms). The maximum spectral width allowed by the hardware was ca. 200 ppm for ^{1}H, so that the extreme low-field signals were recorded in separate runs. Line widths were obtained from the spectra using standard deconvolution procedures. Baseline correction was done carefully for pertinent spectral regions to avoid random errors in the obtained line widths.

Theoretical Calculations. DFT calculations were performed with the Gaussian 98 program.[30] Geometry optimizations were carried out within unconstrained C_1 symmetry. Starting geometries were obtained using molecular mechanics and semiempirical calculations. Becke's three-parameter exchange functional[31] with the gradient-corrected correlation formula of Lee, Yang, and Parr [DFT-(B3LYP)][32] was used with the LANL2DZ basis set.[33] Harmonic vibrational frequencies were calculated using analytical second derivatives (for the Zn systems only). All structures were found to have converged to a minimum on the potential energy surface.

The other calculations were performed using the HyperChem 5.01 program.[34] The standard MM+ force field was used for molecular mechanics, with geometrical restraints imposed on the metal centers to reproduce crystallographically observed bond lengths and angles. Semiempirical calculations were performed at the restricted Hartree−Fock level using the PM3 model.

Acknowledgment. This work was supported by the State Committee for Scientific Research of Poland (KBN) under Grant 4 T09A 147 22 (L.L.-G., M.S., and L.S.). M.S. thanks the Foundation for Polish Science for financial support. DFT calculations were preformed at the Supercomputer Centers in Wrocław and Poznań.

Supporting Information Available: Total electronic energies and coordinates for the DFT optimized structures (a listing in XYZ format). This material is available free of charge via the Internet at http://pubs.acs.org.

IC049172D

(30) Frisch, M. J.; Trucks, G. W.; Schlegel, H. B.; Scuseria, G. E.; Robb, M. A.; Cheeseman, J. R.; Zakrzewski, V. G.; Montgomery, J. A.; Stratmann, R. E.; Burant, J. C.; Dapprich, S.; Millam, J. M.; Daniels, A. D.; Kudin, K. N.; Strain, M. C.; Farkas, O.; Tomasi, J.; Barone, V.; Cossi, M.; Cammi, R.; Mennucci, B.; Pomelli, C.; Adamo, C.; Clifford, S.; Ochterski, J.; Petersson, G. A.; Ayala, P. Y.; Cui, Q.; Morokuma, K.; Malick, D. K.; Rabuck, A. D.; Raghavachari, K.; Foresman, J. B.; Cioslowski, J.; Ortiz, J. V.; Stefanov, B. B.; Liu, G.; Liashenko, A.; Piskorz, P.; Komaromi, I.; Gomperts, R.; Martin, R. L.; Fox, D. J.; Keith, T.; Al-Laham, M. A.; Peng, C. Y.; Nanayakkara, A.; Gonzales, C.; Challacombe, M.; Gill, P. M. W.; Johnson, B. G.; Chen, W.; Wong, M. W.; Andres, J. L.; Head-Gordon, M.; Replogle, E. S.; Pople, J. A. *Gaussian 98*, revision A6; Gaussian, Inc.: Pittsburgh, PA, 1998.

(31) Becke, A. D. *Phys. Rev. A* **1988**, *38*, 3098.
(32) Lee, C.; Yang, W.; Parr, R. G. *Phys. Rev. B* **1988**, *37*, 785.
(33) Hay, P. J.; Wadt, W. R. *J. Chem. Phys.* **1985**, *82*, 270, 284, 299.
(34) *HyperChem, Release 5.01 for Windows. Molecular Modeling System*; Hypercube, Inc.: Gainesville, FL, 1996.